

## Dyes/Pigments

## Soluble Flavanthrone Derivatives: Synthesis, Characterization, and Application to Organic Light-Emitting Diodes

Kamil Kotwica,<sup>[a]</sup> Piotr Bujak,<sup>\*[a]</sup> Przemyslaw Data,<sup>[b, c]</sup> Wojciech Krzywiec,<sup>[a]</sup> Damian Wamil,<sup>[a]</sup> Piotr A. Gunka,<sup>[a]</sup> Lukasz Skorka,<sup>[a]</sup> Tomasz Jaroch,<sup>[d]</sup> Robert Nowakowski,<sup>[d]</sup> Adam Pron,<sup>[a]</sup> and Andrew Monkman<sup>\*[b]</sup>

**Abstract:** Simple modification of benzo[*h*]benz[5,6]acridino[2,1,9,8-*klmna*]acridine-8,16-dione, an old and almost-forgotten vat dye, by reduction of its carbonyl groups and subsequent *O*-alkylation, yields solution-processable, electroactive, conjugated compounds of the periazaacene type, suitable for the use in organic electronics. Their electrochemically determined ionization potential and electron affinity of about 5.2 and  $-3.2$  eV, respectively, are essentially independent of the length of the alkoxy substituent and in good agreement with DFT calculations. The crystal structure of 8,16-dioctyloxybenzo[*h*]benz[5,6]acridino[2,1,9,8-*klmna*]acridine (**FC-8**), the most promising compound, was solved. It crystallizes in space group  $P\bar{1}$  and forms  $\pi$ -stacked columns

held together in the 3D structure by dispersion forces, mainly between interdigitated alkyl chains. Molecules of **FC-8** have a strong tendency to self-organize in monolayers deposited on a highly oriented pyrolytic graphite surface, as observed by STM. 8,16-Dialkoxybenzo[*h*]benz[5,6]acridino[2,1,9,8-*klmna*]acridines are highly luminescent, and all have photoluminescence quantum yields of about 80%. They show efficient electroluminescence, and can be used as guest molecules with a 4,4'-bis(*N*-carbazolyl)-1,1'-biphenyl host in guest/host-type organic light-emitting diodes. The best fabricated diodes showed a luminance of about  $1900 \text{ cd m}^{-2}$ , a luminance efficiency of about  $3 \text{ cd A}^{-1}$ , and external quantum efficiencies exceeding 0.9%.

## Introduction

Organic semiconductors of the acene and azaacene families have been the subject of intensive research interest, mainly due to their good electrical transport properties, which make them interesting materials for applications in field-effect transistors (FETs) and other organic electronic devices.<sup>[1]</sup> Simple acenes and their derivatives such as rubrene (5,6,11,12-tetra-phenyltetracene) and picene (dibenzo[*a,i*]phenanthrene), for example, exhibit very high charge-carrier mobilities compared to other p-type organic semiconductors.<sup>[2]</sup> Thus, acenes are good p-type semiconductors, although their limited stability

towards oxidative degradation should be noted. However, their reduction potential is very low and, as a result, their anion-radical forms are extremely unstable. This excludes the use of acenes as potential n-type semiconductors or ambipolar FETs.<sup>[1a,3]</sup>

Introduction of nitrogen atoms into the fused aromatic structure of acenes drastically changes their redox and electronic properties. Depending on the molecule geometry (linear or nonlinear), the number of nitrogen atoms, and their distribution within the conjugated core, their ionization potential (IP) and electron affinity (EA) can be tuned over a wide range.<sup>[4]</sup> In addition to their interesting electronic properties, photo- and electroluminescence of acenes and azaacenes become possible. These properties make them suitable candidates for use as electroluminophores. The potential importance of these materials was highlighted last year by the decision of the United Nations proclaiming 2015 as the International Year of Light and Light-based Technologies, with the principal goal of searching for new light sources free of toxic elements that, in addition, are less expensive in operation than current ones. In this respect organic materials can easily compete with inorganic counterparts such as nanocrystalline forms of inorganic semiconductors.<sup>[5]</sup> Many acenes<sup>[6]</sup> and azaacenes<sup>[7]</sup> exhibiting high photo- and electroluminescence quantum yields have been reported as the active components of organic light-emitting diodes (OLEDs).

In recent years, synthetic strategies leading to new organic semiconductors in general, and to linear and nonlinear acenes

[a] K. Kotwica, Dr. P. Bujak, W. Krzywiec, D. Wamil, Dr. P. A. Gunka, L. Skorka, Prof. A. Pron  
Faculty of Chemistry, Warsaw University of Technology  
Noakowskiego 3, 00-664 Warsaw (Poland)  
E-mail: piotr.bujak@chem.poczta.onet.pl

[b] Dr. P. Data, Prof. A. Monkman  
Physics Department, University of Durham  
South Road, Durham DH1 3LE (UK)  
E-mail: a.p.monkman@durham.ac.uk

[c] Dr. P. Data  
Faculty of Chemistry, Silesian University of Technology  
M. Strzody 9, 44-100 Gliwice (Poland)

[d] Dr. T. Jaroch, Prof. R. Nowakowski  
Institute of Physical Chemistry, Polish Academy of Science  
Kasprzaka 44/52, 01-224 Warsaw (Poland)

Supporting information for this article is available on the WWW under <http://dx.doi.org/10.1002/chem.201600513>.

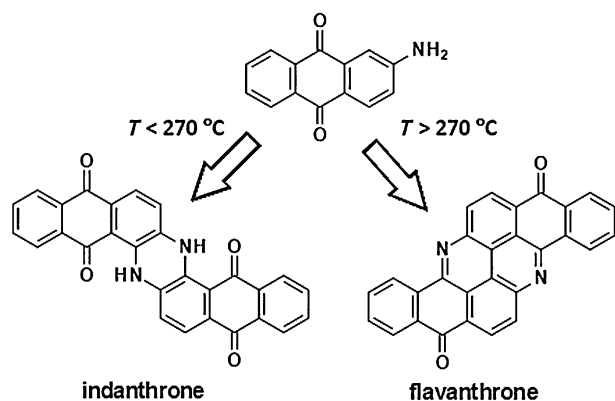
and azaacenes in particular, frequently involved modification of old and sometimes almost-forgotten dyes.<sup>[7d,e,8]</sup> In these cases the target azaacene core was first obtained in one step and then functionalized with solubilizing side groups such as triisopropylsilylethynyl by forming a  $\text{—C}\equiv\text{C—}$  linkage with the core in a second step.<sup>[1]</sup> Compounds in which other groups link the solubilizing side chain with the core, such as  $\text{—CH}_2\text{NH—}$  and  $\text{—CH=N—}$ , were also synthesized.<sup>[9]</sup> Recently, bis-tetracene diketone, first reported in 1949, to which two triisopropylsilylethynyl groups were attached, was used as a substrate in the synthesis of several acenes, and gave good solubility of the functionalized semiconductors in organic solvents.<sup>[10]</sup>

Several substrates known from the synthesis of dyes can also be exploited in the preparation of azaacenes. These include derivatives of aminoanthraquinone or diketopyrrolopyrrole. The synthetic pathway usually involves simple condensation reactions or oxidative C–N coupling, and thus expensive palladium-based catalyst systems can be dispensed with.<sup>[11]</sup>

In the early 1900s, extensive research was carried out on the development of new dyes, one of which was the blue vat dye

6,15-dihydrodinaphtho[2,3-*a*:2',3'-*h*]phenazine-5,9,14,18-tetraone, commonly termed indanthrone, which was synthesized by condensation of aminoanthraquinone at temperatures below 270 °C under basic conditions. Above 270 °C benzo[*h*]benz[5,6]acridino[2,1,9,8-*klmna*]acridine-8,16-dione (flavanthrone), a yellow vat dye, could be obtained from the same substrate (see Scheme 1).

Previously, we transformed indanthrone into a solution-processable organic semiconductors, namely, 5,9,14,18-tetraalkoxydinaphtho[2,3-*a*:2',3'-*h*]phenazines, in a simple one-pot process consisting of the reduction of the carbonyl group by sodium dithionite followed by substitution with solubility-inducing groups under phase-transfer catalysis conditions.<sup>[7d,e]</sup> The resulting compounds showed high photoluminescence quantum yields and could be applied as electroluminophores in guest/host-type LEDs. Herein, we present a systematic study on the synthesis and spectroscopic, structural (including self-assembly), and electrochemical properties of new solution-processable, electroactive, conjugated compounds derived from flavanthrone, and show that in many respects they are distinctly different from the indanthrone derivatives. We also describe guest/host LEDs in which these new electroactive materials are used as electroluminophores.

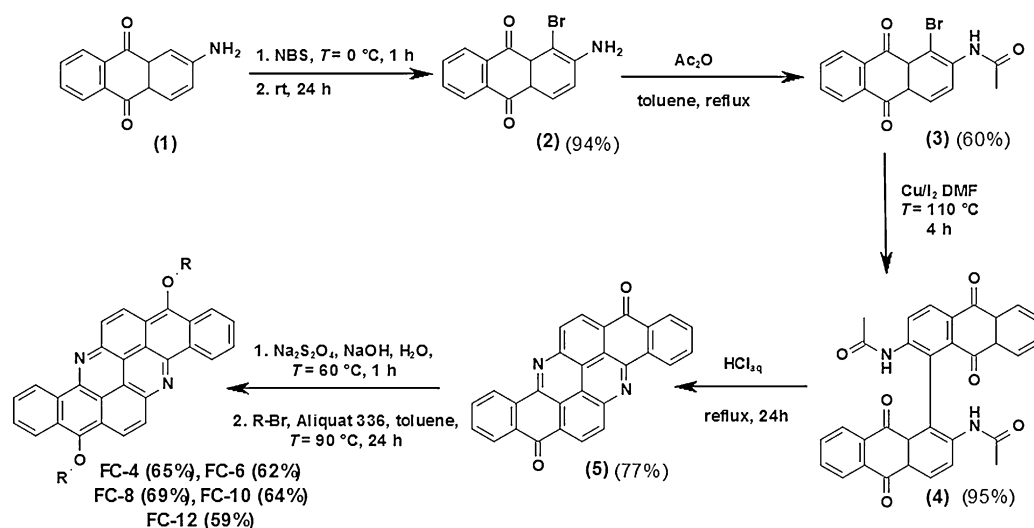


**Scheme 1.** Indanthrone (6,15-dihydrodinaphtho[2,3-*a*:2',3'-*h*]phenazine-5,9,14,18-tetraone) and flavanthrone (benzo[*h*]benz[5,6]acridino[2,1,9,8-*klmna*]acridine-8,16-dione) from aminoanthraquinone.

## Results and Discussion

The synthesis of flavanthrone has been known for over 100 years;<sup>[12]</sup> however, it had to be modified to meet the standards of modern organic chemistry and to improve the reaction yield. Flavanthrone is also commercially available, but requires additional purification when used for the preparation of new semiconductors.

Flavanthrone was obtained from 2-aminoanthraquinone (1), which in the first step was converted to its monobromo derivative 2 by reaction with *N*-bromosuccinimide (NBS) in 1:1 molar ratio (Scheme 2). In the second step, the amino group was protected to yield 3. Then, an Ullmann C–C coupling reac-



**Scheme 2.** Synthetic route to dialkoxy derivatives of benzo[*h*]benz[5,6]acridino[2,1,9,8-*klmna*]acridine-8,16-dione (FC-4–12)

tion was carried out with high yield (95%).<sup>[13]</sup> In the last step a spontaneous reaction of the carbonyl groups with the amino groups took place on deprotection to yield the fused structure of flavanthrone (5).

Flavanthrone was transformed into 8,16-dialkoxybenzo[*h*]-benz[5,6]acridino[2,1,9,8-*klmna*]acridines in a one-pot process, previously elaborated for indanthrone.<sup>[7d]</sup> In the first step the carbonyl groups were reduced to phenolates by using Na<sub>2</sub>S<sub>2</sub>O<sub>4</sub> in sodium hydroxide solution, and then, without the necessity of intermediate product isolation, *O*-alkylation of phenolate groups was performed with alkyl bromides. Application of Na<sub>2</sub>S<sub>2</sub>O<sub>4</sub> as a reducing agent also has a long history, since this reagent was used in coloring fabrics in old procedures employing vat dyes. The reaction pathway is presented in Scheme 2 and the exact preparation procedures can be found the Supporting Information. Five derivatives with increasing alkoxy chain length were synthesized: OC<sub>4</sub>H<sub>9</sub> (**FC-4**), OC<sub>6</sub>H<sub>13</sub> (**FC-6**), OC<sub>8</sub>H<sub>17</sub> (**FC-8**), OC<sub>10</sub>H<sub>21</sub> (**FC-10**), and OC<sub>12</sub>H<sub>25</sub> (**FC-12**).

The <sup>1</sup>H NMR spectrum of **FC-8** is shown in Figure 1a. Since the molecule is symmetrical, in the aliphatic part of the spectrum, at 4.43 ppm, only one triplet (*J* = 6.6 Hz) is observed corresponding to two equivalent OCH<sub>2</sub> groups in the alkoxy substituents. In the aromatic part of the spectrum (Figure 1b) five

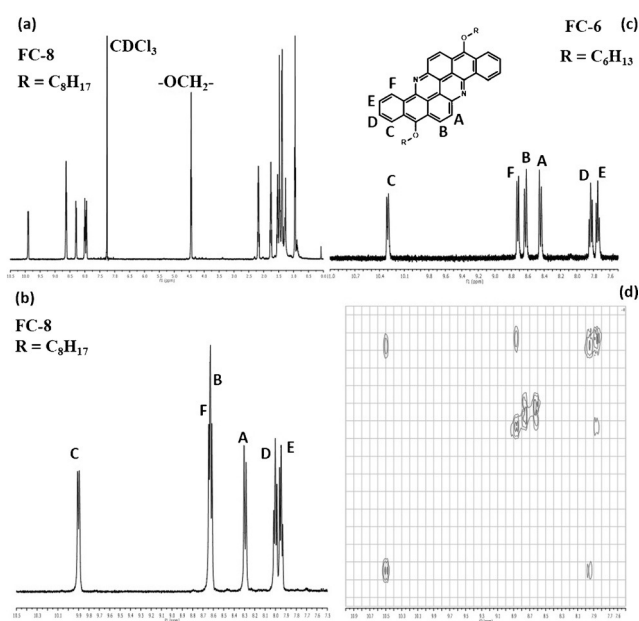


**Figure 1.** <sup>1</sup>H NMR spectra of: a) **FC-8** (whole range), b) **FC-8** (aromatic part), c) **FC-6** (aromatic part), and d) **FC-6** <sup>1</sup>H–<sup>1</sup>H COSY.

signals are observed, although six nonequivalent aromatic protons can be distinguished in the molecular core. This implies that the spectral lines of two nonequivalent protons must overlap. Spectral lines corresponding to six nonequivalent aromatic protons are, however, clearly resolved in the case of **FC-6** (Figure 1c), which greatly facilitates unequivocal assignment of lines, especially as it is supported by the corresponding <sup>1</sup>H–<sup>1</sup>H COSY spectrum (Figure 1d). Two well-resolved doublets at 8.44 and 8.63 ppm (*J* = 9.7 Hz) correspond to H(A) and H(B) of

the diazapyrene core. The doublet at 10.30 ppm (*J* = 8.2 Hz) is attributed to the highly deshielded H(C) proton located in the vicinity of the hexyloxy substituent, and the doublet at 8.77 ppm (*J* = 8.2 Hz) is ascribed to the H(F) proton. These two doublets, despite having the same coupling constant, do not originate from the coupling of H(C) and H(F) protons, as is clearly concluded from the COSY spectrum. The observed chemical shifts of aromatic protons are in very good accordance with the literature data for benzo[*h*]benz[5,6]acridino[2,1,9,8-*klmna*]acridine-8,16-dione containing triisopropylsilylethynyl solubilizing substituents.<sup>[8b]</sup>

Redox properties of the synthesized compounds were studied by cyclic voltammetry. The voltammograms were measured on 5.0 × 10<sup>−4</sup> M solutions in 0.1 M Bu<sub>4</sub>NBF<sub>4</sub>/CH<sub>2</sub>Cl<sub>2</sub> electrolyte and were essentially independent of the length of the alkoxy substituent. Figure 2 shows a representative voltammogram

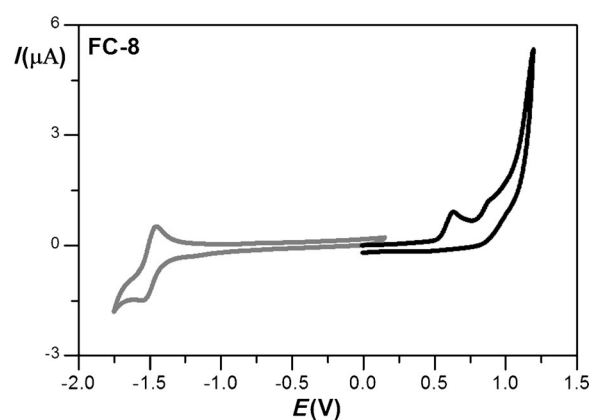


**Figure 2.** Cyclic voltammograms of **FC-8** (electrolyte: 0.1 M Bu<sub>4</sub>NBF<sub>4</sub> in CH<sub>2</sub>Cl<sub>2</sub>, scan rate: 50 mV s<sup>−1</sup>, potential vs. Ag/0.1 M Ag<sup>+</sup>).

for **FC-8**. As reported for alkoxy-substituted dinaphthophenazines (indanthrone derivatives),<sup>[7e]</sup> **FC-8** undergoes an irreversible oxidation at positive potentials (vs. Ag/0.1 M Ag<sup>+</sup>). However, its electrochemical behavior at negative potentials is distinctly different, since a quasireversible redox couple is found for this compound, whereas the reduction of the previously studied alkoxy-substituted dinaphthophenazines is irreversible.

From the onset potentials of the oxidation and reduction peaks (+0.41 and −1.62 V vs. Fc/Fc<sup>+</sup>, respectively) the IP and EA can be calculated by using Equations (1) and (2),<sup>[14]</sup> the results are listed in Table 1.

$$\text{IP/eV} = |e|(E_{\text{ox(onset)}} + 4.8) \quad (1)$$

$$\text{EA/eV} = -|e|(E_{\text{red(onset)}} + 4.8) \quad (2)$$

According to the literature data, flavanthrone (Vat Yellow 1) shows IP = 6.3 eV and |EA| = 3.6 eV.<sup>[15]</sup> The IP of 5.21 eV obtained for **FC-8** is lower than that determined for a tetraoctyloxy derivative of dinaphthophenazine (5.34 eV),<sup>[7e]</sup> whereas |EA| is higher (3.18 and 2.94 eV, respectively). These differences can be considered to

**Table 1.** HOMO and LUMO levels of **FC-8** with corresponding  $E_g$ , IP, and EA calculated at the B3LYP/6-31G(d,p) level of theory. IP and  $|EA|$  values determined by cyclic voltammetry (CV) are shown for comparison. All values are given in electron volts.

| HOMO ( $A_{ij}$ )<br>(vacuum) |
|-------------------------------|-------------------------------|-------------------------------|-------------------------------|-------------------------------|-------------------------------|-------------------------------|-------------------------------|
| -4.95                         | -2.42                         | 5.13                          | 2.61                          | 5.03                          | 2.70                          | 5.21                          | 3.18                          |

be a manifestation of better conjugation within the more fused 4,9-diazapyrene ring compared to the phenazine ring, which facilitates donor–acceptor interactions between the substituent and the *N*-substituted rings. It is also interesting to compare the IP of **FC-8** with that determined electrochemically for a compound with the same molecular core but different solubilizing substituents, namely, triisopropylsilylethynyl groups, reported in ref. [8b]. The latter shows a higher IP (5.36 eV) than **FC-8**, again in accordance with stronger electron-donating properties of the alkoxy group facilitating the oxidation of **FC-8**. No electrochemical data for the reduction process of this triisopropylsilylethynyl derivative are given in ref. [8b].

In polyconjugated systems the first oxidation process leads to the formation of a radical cation, and the first reduction process to a radical anion. It is therefore helpful to analyze these redox processes in connection with the plots of frontier orbitals and spin-density distribution of the radical ions formed (Figure 3). Both HOMO and LUMO occupy the central fused aromatic core of the molecule, that is, the HOMO is located mainly on the edge of this skeleton with the highest contribution from the carbon atom attached to the oxygen atom of the alkoxy substituent and with zero contribution from the two central carbon atoms. The LUMO, on the other hand, is located more towards the central part of the molecule and also has strong contributions from the aforementioned CO carbon and nitrogen atoms. The spin-density distributions in the radi-

cal ions show a similar behavior. The spin density of the radical cation is mainly located in the proximity of the CO carbon atom, with no contribution from the central part of the ring, whereas in the radical anion it additionally occupies the space near the nitrogen atoms.

DFT calculations also enable the determination of the IP and EA values of isolated molecules and molecules in solution, in the latter case by using the polarizable continuum model (PCM). IP and EA values of **FC-8** were calculated for a solution in dichloromethane, that is, the solvent that was used in the determination of the same parameters by cyclic voltammetry (Table 1). Better agreement between the theoretical and experimental values was obtained for the IP, and EA values differed by 0.48 eV. However, compared to indanthrone, the overall match between theory and experiment is far better.

Solution absorption and emission spectra of the various derivatives are essentially independent of the length of the alkoxy substituent. Figure 4 shows the spectra of **FC-8** as a representative example, and those of the other derivatives are collected in the Supporting Information. These spectra show features typical of periacenes and periazaacenes,<sup>[8b,10,16]</sup> which usually show a set of absorption bands originating from  $\pi \rightarrow \pi^*$  and  $n \rightarrow \pi^*$  transitions, which are bathochromically shifted with increasing size of the aromatic core.<sup>[4c,17]</sup> Pronounced vibronic character of the lowest-energy band (at 515 nm for the 0–0 transition) is notable. The spectrum is consistent with the cal-

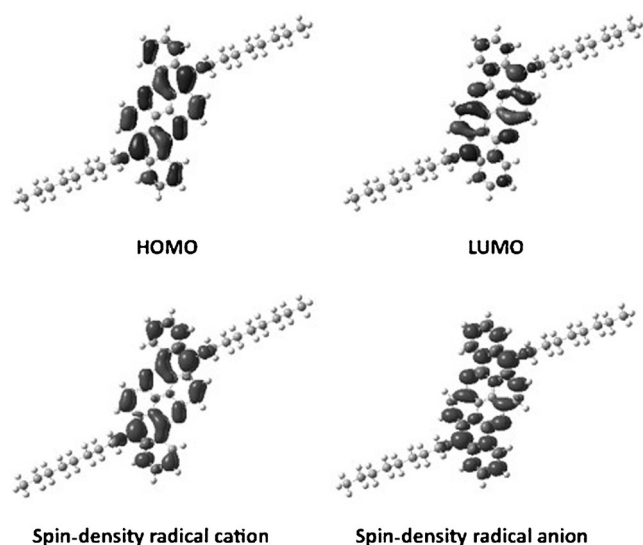


**Figure 3.** Frontier molecular orbital plots for **FC-8** (top: isosurface value = 0.03) and spin densities for radical cation and anion forms of this compound (bottom: isosurface value = 0.001).

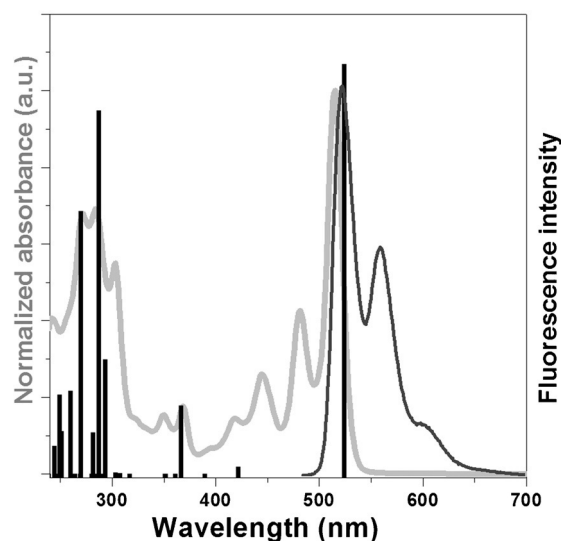


**Figure 4.** Absorption and emission spectra of **FC-8** (chloroform as solvent). The calculated positions and relative oscillator strengths of the electronic transitions of this compound, obtained from TDDFT calculations, are depicted as black bars for comparison.

culated transitions (see Figure 4 and Table S2 in the Supporting Information). The strongest band at 515 nm is almost purely HOMO (H)→LUMO (L) in nature (98%). This transition is favored in centrosymmetric ( $C_2$  point group) molecules such as **FC-8**, since the frontier orbitals (HOMO and LUMO) by symmetry belong to two different irreducible representations  $A_u$  and  $A_g$ , respectively, and the H→L transition is highly allowed according to the Laporte selection rule. Full analysis of the electronic transition can be found in the Supporting Information.

The optical bandgap  $E_{g,opt}$  of **FC-8**, determined from the onset of the lowest-energy absorption band, is 2.33 eV, that is, 100 meV larger than that of isopropylsilylethynyl-functionalized periazaacene with the same core.<sup>[8b]</sup> However, it is 70 meV smaller than the that of 5,9,14,18-tetraoctyloxynaphtho[2,3-*a*:2',3'-*h*]phenazine (the corresponding indanthrone derivative).<sup>[7e]</sup>

All compounds of the **FC-*n*** series exhibit strong green photoluminescence. Their emission spectra can be treated as mirror images of the absorption spectra (see Figure 4, in which the emission and absorption spectra of **FC-8** are shown as an example). This feature, together with a very small Stokes shift of 9 nm, clearly indicates a very similar molecular geometry in the ground and excited states, consistent with the rigid nature of the core. The experimental emission wavelength corresponds very well with that calculated by state-specific TDDFT ( $\lambda_{em} = 554$  nm). The measured photoluminescence quantum yield (PLQY) in all cases reaches 80%, a value which is significantly higher than those measured for tetraalkoxydinaphthophenazines, that is, the corresponding indanthrone derivatives (ca. 60%).<sup>[7e]</sup>

As with tetraalkoxydinaphthophenazines,<sup>[8b]</sup> compounds of the **FC-*n*** series are capable of self-assembling into highly ordered 2D supramolecular structures in monolayers deposited on suitable substrates such as highly oriented pyrolytic graphite (HOPG). Figure 5a and b show representative STM images

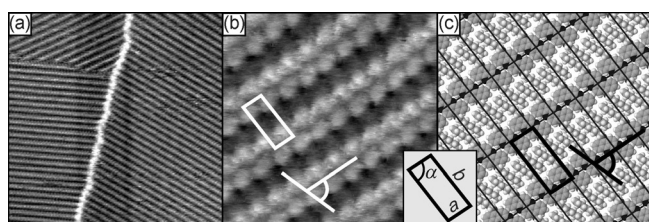


**Figure 5.** a), b) STM images and c) proposed adsorption geometry of a monolayer of **FC-8** on HOPG. Scanning area and parameters: a)  $61 \times 61$  nm, b)  $9 \times 9$  nm<sup>2</sup>,  $V_{bias} = 1$  V,  $I_t = 0.3$  nA.

of a monolayer of **FC-8** deposited on a HOPG substrate. The adsorbate molecules are well-organized into large domains with typical size of a few hundred nanometers, which differ in their orientation (see upper part of the large-scale image in Figure 5a). Each domain is observed by STM as a set of parallel bright stripes corresponding to rows of molecules oriented in one direction.

Images obtained at higher magnification (Figure 5b) provide more detailed information concerning the arrangement of indi-

vidual molecules in the monolayer. Each stripe, clearly visible in this image, is characterized by its inner structure, which consists of two rows of well-resolved bright spots. It is expected that this signal of higher tunneling current corresponds to the conjugated cores of the investigated adsorbate. Microscopic investigations performed with different bias potentials (not discussed here) enabled us to postulate the orientation of molecules in the observed rows. This direction ( $70^\circ$  with respect to the direction of the row orientation) is marked schematically in Figure 5b by an angle indicated in white. Each molecule is therefore visible at submolecular resolution as a set of two bright spots oriented along this axis. The 2D unit-cell parameters determined from the STM images are:  $0.91 \pm 0.05$  nm/ $2.30 \pm 0.1$  nm/ $84 \pm 2^\circ$ . The corresponding model of the adsorption geometry is presented in Figure 5c. The dimension of the unit cell along its shorter axis (0.91 nm) indicates that the fused aromatic cores of adjacent molecules are tightly packed in this direction. This correlation also shows that in the monolayer the conjugated cores of the molecules lie flat on the substrate surface. The molecular rows formed in this way are separated by a distance of 2.30 nm imposed by the interdigitation of alkyl substituents.

We further investigated the self-organized 2D pattern to determine how the observed monolayer structure of **FC-8** is related to its 3D organization in a single crystal. Crystal structure analysis revealed that **FC-8** crystallizes in triclinic space group  $P\bar{1}$ . The molecule consists of a flat aromatic core and two *n*-octyloxy groups in the *anti* conformation (see Figure 6 for the molecular structure of **FC-8**). The root mean square displacement of atoms constituting the aromatic core from the mean plane is 0.052 Å, and the C29-O1-O2-C37 torsion angle describing the mutual orientation of alkoxy groups is  $178.8(3)^\circ$ . Inversion-related molecules form dimers through  $\pi$  stacking accompanied by C–H...O interactions (Figure 7,  $d(C29 \cdots O2) = 3.332(4)$  Å,  $d(H29B \cdots O2) = 2.44$  Å,  $C29-H29B \cdots O2 = 150^\circ$ ,  $i = 1-x$ ,

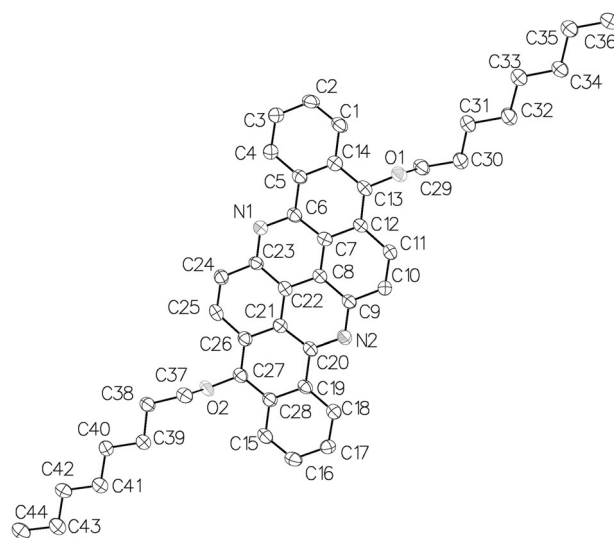


**Figure 6.** Molecular structure of **FC-8** with atom numbering scheme. Thermal ellipsoids drawn at 50% probability and hydrogen atoms omitted for clarity.

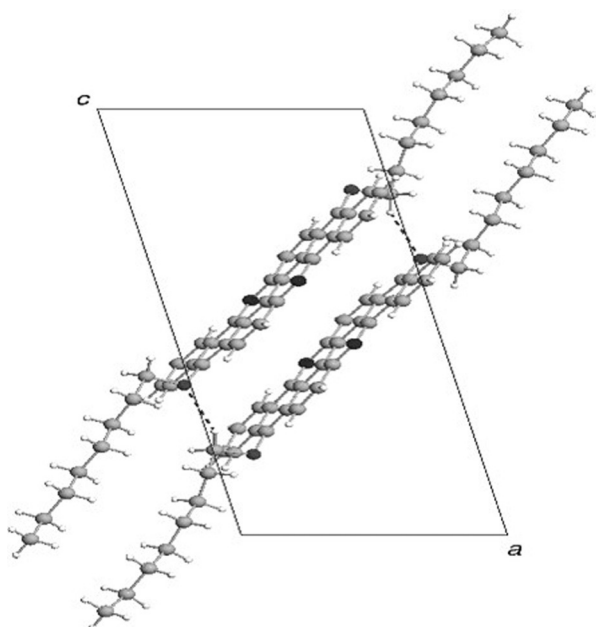


**Figure 7.** Unit cell of **FC-8** (ball-and-stick model) viewed along the [010] direction. C–H...O hydrogen bonds are shown as dashed lines.

1–*y*, 1–*z*). The dimers in turn form  $\pi$ -stacked columns running along the [100] direction (Figure S2 in the Supporting Information). The distance between mean planes of the aromatic cores in the dimers is 3.4398(11) Å with a plane shift of 1.7825(12) Å, while the interplanar distance between molecules from the adjacent dimers is 3.3030(15) Å, but the plane shift is 7.8503(14) Å (Figure S2 in the Supporting Information). Columns are held together in the 3D structure by dispersion forces, mainly between interdigitated alkyl chains. In this crystalline arrangement it is possible to identify almost flat and densely packed slices of molecules with 2D ordering very similar to that found in the monolayer deposited on HOPG (Figure S3 in Supporting Information). The 2D unit-cell parameters of the slice are 0.9365(4) nm/2.3929(4) nm/86.86(2)°, which confirm the unit-cell parameters of the monolayer determined from STM measurements (corresponding parameters: 0.91 ± 0.05 nm/2.30 ± 0.1 nm/84 ± 2°).

The triisopropylsilylethynyl-substituted analogue of the **FC-*n*** series of compounds also readily forms single crystals, and hence it was used in the fabrication of single-crystal FETs showing reasonable hole mobility.<sup>[8b]</sup> Considering the excellent luminescent properties of all **FC-*n*** derivatives (PLQY of 80%), we explored their application as high-mobility electrolumino-phores in OLEDs, especially in view of the fact that such applications are extremely rare in the case of azaacenes and periazaacenes.<sup>[7d–f, 18]</sup>

The device structure used for guest/host-type diodes was ITO/PEDOT:PSS/PVK/(**FC-4,8,12**)-CBP/TPBi/LiF/Al. The corresponding energy-level scheme for this structure is shown in Figure 8a. The emissive layer was varied over a range of emitter concentrations of 1–15% of a given **FC-*n*** compound molecularly dispersed in a 4,4'-bis(*N*-carbazolyl)-1,1'-biphenyl (CBP) matrix. This emissive layer was sandwiched between a hole-

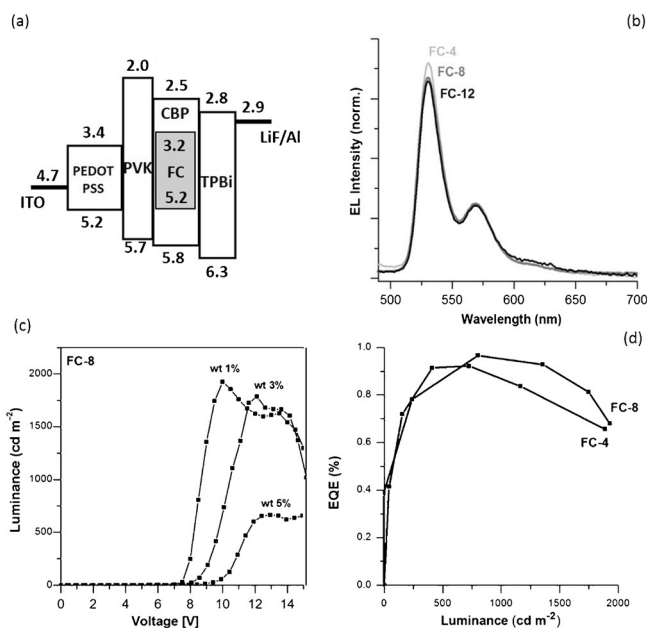


**Figure 8.** a) Device structure and energy diagram of the green LED. b) Electroluminescence spectra of 1 wt% dispersion of **FC-4**, **FC-8**, and **FC-12** in CPB matrix. c) Luminance versus voltage characteristics for diodes with active layers containing increasing amounts of **FC-8**: 1, 3, and 5%. d) External quantum efficiency versus luminance characteristics for OLEDs with **FC-4** and **FC-8** (1 wt%).

transporting layer of poly(9-vinylcarbazole) (PVK) and a hole-blocking layer of 2,2',2''-(1,3,5-benzinetriyl)-tris(1-phenyl-1*H*-benzimidazole) (TPBi) by a hybrid solution/vacuum codeposition method. These two layers were separated from the electrodes (indium tin oxide (ITO) and Al) by layers of poly(3,4-ethylenedioxythiophene):polystyrene sulfonate (PEDOT:PSS) and LiF, respectively.

Figure 8b shows the electroluminescence spectra measured for the emissive layer containing 1% of the **FC-*n*** luminophore. These spectra resemble the photoluminescence spectra recorded from chloroform solutions of the studied luminophores, with retention of the vibrational structure but the emission peaks bathochromically shifted by 10–15 nm (cf. Figures 4 and 8b). Figure 8c shows plots of luminance versus voltage for increasing contents of **FC-8** luminophore in the CBP matrix. Clearly, with increasing content of the electrolumino-phore the luminance decreases with simultaneous increase of the turn-on voltage. This may suggest nanoaggregation occurring at higher electrolumino-phore contents, which favors nonradiative quenching of the emitter. The parameters of all studied diodes are listed in Table 2. The highest luminance values (approaching 1900 cd m<sup>-2</sup>) were obtained for **FC-4** and **FC-8**, whereas the highest luminous efficiency (> 3 cd A<sup>-1</sup>) was found for **FC-8**. In the case of **FC-4** and **FC-8** the highest external quantum efficiencies (EQEs), exceeding 0.9%, were measured for moderate luminances, but they never dropped below 0.65% for the whole range of luminances studied (see Figure 8d).

**Table 2.** Electroluminescence data for diodes containing **FC-4**, **FC-8**, and **FC-12** (1–15 wt%) as electroluminophores.

| c [wt%] | <b>FC-4</b>                      |                                   | <b>FC-8</b>                |                             | <b>FC-12</b>               |                             |
|---------|----------------------------------|-----------------------------------|----------------------------|-----------------------------|----------------------------|-----------------------------|
|         | $L^{[a]}$ [ $\text{cd m}^{-2}$ ] | $LE^{[b]}$ [ $\text{cd A}^{-1}$ ] | $L$ [ $\text{cd m}^{-2}$ ] | $LE$ [ $\text{cd A}^{-1}$ ] | $L$ [ $\text{cd m}^{-2}$ ] | $LE$ [ $\text{cd A}^{-1}$ ] |
| 1       | 1885                             | 2.74                              | 1860                       | 3.06                        | 1460                       | 2.13                        |
| 3       | 988                              | 1.21                              | 1790                       | 1.17                        | 1580                       | 1.63                        |
| 5       | 1100                             | 0.96                              | 717                        | 0.34                        | 262                        | 0.12                        |
| 10      | 746                              | 0.66                              | 619                        | 0.39                        | 54                         | 0.23                        |
| 15      | 500                              | 0.29                              | –                          | –                           | 155                        | 0.16                        |

[a] Luminance. [b] Luminous efficiency.

## Conclusion

We have demonstrated that by simple modification of benzo[*h*]benz[5,6]acridino[2,1,9,8-*klmna*]acridine-8,16-dione (flavanthrone), an old, intractable, and almost-forgotten vat dye, through reduction of its carbonyl groups to phenolates followed by their *O*-alkylation, it is possible to obtain a new group of solution-processable, electroactive, conjugated compounds, namely, 8,16-dialkoxybenzo[*h*]benz[5,6]acridino[2,1,9,8-*klmna*]acridines. HOMO and LUMO energies of these compounds as well as their IPs and EAs make them suitable candidates for application as components of organic FETs and LEDs. The latter possibility was explored, and green-emitting diodes were obtained in a guest/host configuration with CBP host. Self-assembly of these compounds resulted in formation of monolayers on the surface of HOPG, in which highly ordered 2D supramolecular organization extends over a few hundred nanometers.

## Experimental Section

### Synthesis

A list of all chemicals, detailed descriptions of the synthesis of all investigated compounds, and spectroscopic characterization data can be found in the Supporting Information.

### Spectroscopy

$^1\text{H}$  NMR and  $^{13}\text{C}$  NMR spectra were recorded with a Varian Unity Inova 500 MHz spectrometer and referenced to TMS or solvents. The elemental analyses were carried out with a Vario EL III (Elementar) CHN analyzer. HRMS spectra were recorded in methanol with Mariner ESI-TOF (Applied Biosystems) mass spectrometer. Solution UV/Vis/NIR spectra were recorded in chloroform with a Cary 5000 (Varian) spectrometer, and the emission spectra with an Edinburgh FS 900 CDT fluorometer (Edinburgh Analytical Instruments). Photoluminescence quantum yields were determined by using quinine sulfate in 0.05 mol dm $^{-3}$  H $_2$ SO $_4$  ( $\varphi_{\text{fl}} = 0.51$ ) as standard.<sup>[19]</sup>

### Cyclic Voltammetry

Cyclic voltammetry was performed in a three-electrode, one-compartment cell with a platinum working electrode (3 mm $^2$ ), a platinum-wire counter electrode, and a Ag/0.1 M AgNO $_3$ /CH $_3$ CN reference electrode. A given flavanthrone derivative was dissolved in 0.1 M Bu $_4$ NBF $_4$  in dichloromethane to yield a 5  $\times$  10 $^{-4}$  M solution.

## Computational Methods

DFT calculations were carried out with the Gaussian 09 Revision D.01<sup>[20]</sup> package by employing the B3LYP<sup>[21]</sup> hybrid exchange correlation functional and 6-31G(d,p) basis set. Ground- and excited-state geometries were fully optimized until a stable local minimum was found, which was confirmed by normal-mode analysis (no imaginary frequencies were present). Initial structures were constrained to the  $C_1$  symmetry point group and then relaxed if a saddle point was found. Solvent–solute interactions were taken into account with the aid of the PCM model<sup>[22]</sup> and dichloromethane as solvent. The oscillator strengths and energies of the vertical singlet excitations were calculated by employing the time-dependent (TD) version of DFT<sup>[23]</sup> at respective optimized geometries. Multiconfigurational character of the most pronounced excitations was analyzed with Natural Transition Orbitals (NTO).<sup>[24]</sup> Excited-to-ground state transitions were calculated by the state-specific solvation approach taking into account the Franck–Condon rule.<sup>[25]</sup> The necessary data of DFT calculations were retrieved from output files by using GaussSum 2.2.<sup>[26]</sup> All necessary initial geometries and final graphics (molecular orbitals and spin densities) were generated in GaussView 5.0.<sup>[27]</sup>

## Scanning tunneling microscopy

Monomolecular layers were prepared by drop casting from a solution of the investigated compound in hexane ( $\approx 2 \text{ mg L}^{-1}$ ) on a freshly cleaved HOPG surface (SPI Supplies, USA). The layers were dried under ambient conditions and then imaged in air at room temperature with an STM system (University of Bonn, Germany).<sup>[28]</sup> All images were recorded in constant-current mode with mechanically cut Pt/Ir (80/20%) tips. The proposed real-space models of the monomolecular layers were obtained by correlation of the layer structure deduced from the STM images and the molecular model of the investigated adsorbate determined by using the HyperChem software package.

## X-ray diffraction

A suitable single crystal of **FC-8**, grown from chlorobenzene, was selected under a polarizing microscope, mounted in inert oil (Paratone N), and transferred to the cold gas stream of the diffractometer. Diffraction data were collected with an Oxford Diffraction  $\kappa$ -CCD Gemini A Ultra diffractometer at 120(2) K with mirror-focused Cu $_{\text{K}\alpha}$  radiation. Cell refinement and data collection, reduction, and analysis were performed with the CrysAlis<sup>PRO</sup> software.<sup>[29]</sup> The structures were solved by direct methods and subsequent Fourier-difference synthesis with SHELXT and refined by full-matrix, least-squares methods against  $F^2$  with SHELXL-2014 within the Olex2 program suite.<sup>[30]</sup> All non-hydrogen atoms were refined anisotropically. Hydrogen atoms were introduced at calculated positions and refined as riding atoms. Data were analyzed with Olex2, Platon, and Diamond.<sup>[30b,31]</sup> Crystal data and structure refinement parameters are given in Table S3 of the Supporting Information. Images were created using Olex2 and Diamond and were rendered with POV-Ray.<sup>[30b,31b,32]</sup>

## Electroluminescence measurements and LED fabrication

Guest/host-type electroluminescent diodes were fabricated by molecular dispersion of **FC-4**, **FC-8**, or **FC-12** (1 to 15 wt%) in an one-component matrix consisting of 4,4'-bis(*N*-carbazolyl)-1,1'-biphenyl

(CBP). Poly(9-vinylcarbazole) (PVK) and 2,2',2''-(1,3,5-benzinetriyl)-tris(1-phenyl-1-H-benzimidazole) (TPBi) were used as hole-transporting layer and hole-blocking layer, respectively. The active layer of about 50 nm was deposited on top of an ITO electrode pre-coated with a PEDOT:PSS layer of about 50 nm thickness and with a PVK layer of about 10 nm thickness. In the subsequent step a TPBi (50 nm) layer and an ultrathin (1 nm) LiF layer were evaporated followed by deposition of an Al layer. The fabricated devices were tested under ambient conditions. Characteristics of OLED devices were measured in a ten-inch integrating sphere (Labsphere) connected to a Source Meter Unit (and calibrated with NIST calibration lamp)

## Acknowledgements

K.K., P.B., L.S., and A.P. wish to acknowledge financial support from the Foundation for the Polish Science Team Programme cofinanced by the EU European Regional Development Fund. (Contract No. TEAM/2011-8/6). P.B. and A.P. additionally acknowledge financial support from the National Science Centre of Science in Poland (NCN, Grant No. 2015/17/B/ST5/00179).

**Keywords:** alkylation · dyes/pigments · luminescence · self-assembly · semiconductors

- [1] a) J. E. Anthony, *Angew. Chem. Int. Ed.* **2008**, *47*, 452–483; *Angew. Chem.* **2008**, *120*, 460–492; b) U. H. F. Bunz, J. U. Engelhart, B. D. Lindner, M. Schaffroth, *Angew. Chem. Int. Ed.* **2013**, *52*, 3810–3821; *Angew. Chem.* **2013**, *125*, 3898–3910; c) C. Wang, P. Gu, B. Hu, Q. Zhang, *J. Mater. Chem. C* **2015**, *3*, 10055–10065; d) J. Li, Q. Zhang, *ACS Appl. Mater. Interfaces* **2015**, *7*, 28049–28062.
- [2] a) V. C. Sundar, J. Zaumseil, V. Podzorov, E. Menard, R. L. Willett, T. Sorneyka, M. E. Gershenson, J. A. Roger, *Science* **2004**, *303*, 1644–1646; b) H. Okamoto, N. Kwasaki, Y. Kaji, Y. Kubozono, A. Fujiwara, M. Yamaji, *J. Am. Chem. Soc.* **2008**, *130*, 10470–10471.
- [3] J. E. Anthony, *Chem. Rev.* **2006**, *106*, 5028–5048.
- [4] a) Z. Liang, Q. Tang, R. Mao, D. Liu, J. Xu, Q. Miao, *Adv. Mater.* **2011**, *23*, 5514–5518; b) Y. Sakamoto, T. Suzuki, M. Kobayashi, Y. Gao, Y. Fukai, Y. Inoue, F. Sato, S. Tokito, *J. Am. Chem. Soc.* **2004**, *126*, 8138–8140; c) Z. Liang, Q. Tang, J. Xu, Q. Miao, *Adv. Mater.* **2011**, *23*, 1535–1539; d) Q. Miao, *Adv. Mater.* **2014**, *26*, 5541–5549; e) C. Wang, J. Zhang, G. Long, N. Aratani, H. Yamada, Y. Zhao, Q. Zhang, *Angew. Chem. Int. Ed.* **2015**, *54*, 6292–6296; *Angew. Chem.* **2015**, *127*, 6390–6394.
- [5] S. Reineke, *Nat. Mater.* **2015**, *14*, 459–462.
- [6] a) J. Xiao, S. Liu, Y. Liu, L. Ji, X. Liu, H. Zhang, X. Sun, Q. Zhang, *Chem. Asian J.* **2012**, *7*, 561–564; b) Q. Zhang, Y. Divayana, J. Xiao, Z. Wang, E. R. T. Tiekink, H. M. Duong, H. Zhang, F. Boey, X. W. Sun, F. Wudl, *Chem. Eur. J.* **2010**, *16*, 7422–7426; c) J. Xiao, Y. Divayana, Q. Zhang, H. M. Duong, H. Zhang, F. Boey, X. W. Sun, F. Wudl, *J. Mater. Chem.* **2010**, *20*, 8167–8170.
- [7] a) C. Fu, M. Li, Z. Su, Z. Hong, W. Li, B. Li, *Appl. Phys. Lett.* **2006**, *88*, 093507; b) X. Xu, G. Yu, S. Chen, C. Di, Y. Liu, *J. Mater. Chem.* **2008**, *18*, 299–305; c) K.-i. Nakayama, Y. Hashimoto, H. Sasabe, Y.-J. Pu, M. Yokoyama, J. Kido, *Jpn. J. Appl. Phys.* **2010**, *49*, 01AB11; d) K. Kotwica, P. Bujak, D. Wamil, M. Materna, L. Skorka, P. A. Gunka, R. Nowakowski, B. Golec, B. Luszczynska, M. Zagorska, A. Pron, *Chem. Commun.* **2014**, *50*, 11543–11546; e) K. Kotwica, P. Bujak, D. Wamil, A. Pieczonka, G. Wiosna-Salyga, P. A. Gunka, T. Jaroch, R. Nowakowski, B. Luszczynska, E. Witkowska, I. Glowacki, J. Ulanski, M. Zagorska, A. Pron, *J. Phys. Chem. C* **2015**, *119*, 10700–10708; f) P.-Y. Gu, Y. Zhao, J.-H. He, J. Zhang, C. Wang, Q.-F. Xu, J.-M. Lu, X. W. Sun, Q. Zhang, *J. Org. Chem.* **2015**, *80*, 3030–3035.
- [8] a) L. Zhang, B. Walker, F. Liu, N. S. Colella, S. C. B. Mannsfeld, J. J. Watkins, T.-Q. Nguyen, A. L. Briseno, *J. Mater. Chem.* **2012**, *22*, 4266–4268; b) L. Zhang, A. Fonari, Y. Zhang, G. Zhao, V. Coropceanu, W. Hu, S. Parkin, J.-L. Brédas, A. L. Briseno, *Chem. Eur. J.* **2013**, *19*, 17907–17916; c) M. K. Węclawski, M. Tasiar, T. Hammann, P. J. Cywiński, D. T. Gryko, *Chem. Commun.* **2014**, *50*, 9105–9108.
- [9] J.-B. Giguère, J.-F. Morin, *J. Org. Chem.* **2013**, *78*, 12769–12778.
- [10] L. Zhang, A. Fonari, Y. Liu, A.-L. M. Hoyt, H. Lee, D. Granger, S. Parkin, T. P. Russell, J. E. Anthony, J.-L. Brédas, V. Coropceanu, A. L. Briseno, *J. Am. Chem. Soc.* **2014**, *136*, 9248–9251.
- [11] a) K. Goto, R. Yamaguchi, S. Hirato, H. Ueno, T. Kawai, H. Shinokubo, *Angew. Chem. Int. Ed.* **2012**, *51*, 10333–10336; *Angew. Chem.* **2012**, *124*, 10479–10482; b) W. Yue, S.-L. Suraru, D. Bialas, M. Müller, F. Würthner, *Angew. Chem. Int. Ed.* **2014**, *53*, 6159–6162; *Angew. Chem.* **2014**, *126*, 6273–6276; c) D. Sakamaki, D. Kumano, E. Yashima, S. Seki, *Angew. Chem. Int. Ed.* **2015**, *54*, 5404–5407; *Angew. Chem.* **2015**, *127*, 5494–5497.
- [12] R. Scholl, H. Berblinger, *Chem. Ber.* **1903**, *36*, 3427–3445.
- [13] a) A. Schuhmacher, Deutsche Patent, DPMA DE1955157; b) B. Rastoin, Deutsche Patent, DPMA DE1944276.
- [14] a) S. Trasatti, *Pure Appl. Chem.* **1986**, *58*, 955–966; b) C. M. Cardona, W. Li, A. E. Kaifer, D. Stockdale, G. C. Bazan, *Adv. Mater.* **2011**, *23*, 2367–2371; c) R. Rybakiewicz, P. Gawrys, D. Tsikritzis, K. Emmanouil, S. Kennou, M. Zagorska, A. Pron, *Electrochim. Acta* **2013**, *96*, 13–17.
- [15] E. D. Glowacki, L. Leonat, G. Voss, M. Bodea, Z. Bozkurt, M. Irima-Vladu, S. Bauer, N. S. Sariciftci, *Proc. SPIE-Int. Soc. Opt. Eng.* **2011**, *8118*, 81180M.
- [16] E. Ahmed, A. L. Briseno, Y. Xia, S. A. Jenekhe, *J. Am. Chem. Soc.* **2008**, *130*, 1118–1119.
- [17] S. Miao, A. L. Appleton, N. Berger, S. Barlow, S. R. Marder, K. I. Hardcastle, U. H. F. Bunz, *Chem. Eur. J.* **2009**, *15*, 4990–4993.
- [18] B. D. Lindner, Y. Zhang, S. Höfle, N. Berger, C. Teusch, M. Jesper, K. I. Hardcastle, X. Qian, U. Lemmer, A. Colmann, U. H. F. Bunz, M. Hamburger, *J. Mater. Chem. C* **2013**, *1*, 5718–5724.
- [19] R. A. Velapoldi, Proceedings on the 1972 Conference on Accuracy in Spectrophotometry and Luminescence Measurements, National Bureau of Standards Special Publ. 378; U. S. Govt. Print Office, Washington, DC, 1973; p. 231.
- [20] Gaussian 09, Revision D.01, M. J. Frisch, G. W. Trucks, H. B. Schlegel, G. E. Scuseria, M. A. Robb, J. R. Cheeseman, G. Scalmani, V. Barone, B. Mennucci, G. A. Petersson, H. Nakatsuji, M. Caricato, X. Li, H. P. Hratchian, A. F. Izmaylov, J. Bloino, G. Zheng, J. L. Sonnenberg, M. Hada, M. Ehara, K. Toyota, R. Fukuda, J. Hasegawa, M. Ishida, T. Nakajima, Y. Honda, O. Kitao, H. Nakai, T. Vreven, J. A. Montgomery, Jr., J. E. Peralta, F. Ogliaro, M. Bearpark, J. J. Heyd, E. Brothers, K. N. Kudin, V. N. Staroverov, R. Kobayashi, J. Normand, K. Raghavachari, A. Rendell, J. C. Burant, S. S. Iyengar, J. Tomasi, M. Cossi, N. Rega, J. M. Millam, M. Klene, J. E. Knox, J. B. Cross, V. Bakken, C. Adamo, J. Jaramillo, R. Gomperts, R. E. Stratmann, O. Yazyev, A. J. Austin, R. Cammi, C. Pomelli, J. W. Ochterski, R. L. Martin, K. Morokuma, V. G. Zakrzewski, G. A. Voth, P. Salvador, J. J. Dannenberg, S. Dapprich, A. D. Daniels, Ö. Farkas, J. B. Foresman, J. V. Ortiz, J. Cioslowski, D. J. Fox, Gaussian, Inc. Wallingford CT, **2013**.
- [21] a) A. D. Becke, *J. Chem. Phys.* **1993**, *98*, 1372–1377; b) A. D. Becke, *J. Chem. Phys.* **1993**, *98*, 5648–5652; c) C. T. Lee, W. T. Yang, R. G. Parr, *Phys. Rev. B* **1988**, *37*, 785–789.
- [22] J. Tomasi, B. Mennucci, R. Cammi, *Chem. Rev.* **2005**, *105*, 2999–3093.
- [23] a) R. Bauernschmitt, R. Ahlrichs, *Chem. Phys. Lett.* **1996**, *256*, 454–464; b) M. E. Casida, C. Jamorski, K. C. Casida, D. R. Salahub, *J. Chem. Phys.* **1998**, *108*, 4439–4449; c) R. E. Stratmann, G. E. Scuseria, M. J. Frisch, *J. Chem. Phys.* **1998**, *109*, 8218–8224; d) C. van Caillie, R. D. Amos, *Chem. Phys. Lett.* **1999**, *308*, 249–255; e) C. van Caillie, R. D. Amos, *Chem. Phys. Lett.* **2000**, *317*, 159–164; f) F. Furche, R. Ahlrichs, *J. Chem. Phys.* **2002**, *117*, 7433–7447; g) G. Scalmani, M. J. Frisch, B. Mennucci, J. Tomasi, R. Cammi, V. Barone, *J. Chem. Phys.* **2006**, *124*, 094107-1-094107-15.
- [24] R. L. Martin, *J. Chem. Phys.* **2003**, *118*, 4775–4777.
- [25] a) R. Improta, V. Barone, G. Scalmani, M. J. Frisch, *J. Chem. Phys.* **2006**, *125*, 054103-1-054103-9; b) R. Improta, G. Scalmani, M. J. Frisch, V. Barone, *J. Chem. Phys.* **2007**, *127*, 074504-1-074504-9.
- [26] N. M. O'Boyle, A. L. Tenderholt, K. M. Langner, *J. Comput. Chem.* **2008**, *29*, 839–845.
- [27] R. Dennington, T. Keith, J. Millam, *GaussView*, Version 5, Semichem Inc., Shawnee Mission, KS, **2009**.
- [28] M. Wilmis, M. Kruff, G. Bermes, K. Wandelt, *Rev. Sci. Instrum.* **1999**, *70*, 3641–3650.
- [29] *CrysAlisPro Software system ver. 171.37.35*, Agilent Technologies UK Ltd, Oxford, UK, **2014**.

- [30] a) G. M. Sheldrick, *Acta Crystallogr. Sect. A* **2015**, *71*, 3–8; b) O. V. Dolomanov, L. J. Bourhis, R. J. Gildea, J. A. K. Howard, H. Puschmann, *J. Appl. Crystallogr.* **2009**, *42*, 339–341.
- [31] a) A. L. Spek, *J. Appl. Crystallogr.* **2003**, *36*, 7–13; b) *Diamond ver. 3.2k*, Crystal Impact GbR, Bonn, **2014**.

- [32] *Persistence of Vision (TM) Raytracer (POV-RAY)*, Persistence of Vision Pty. Ltd, Williamstown, Victoria, **2010**.

---

Received: February 3, 2016

Published online on April 23, 2016